

EUV-TEC - an index to describe ionospheric variability using satellite-borne solar EUV measurements: first results

C. Unglaub¹, Ch. Jacobi¹, G. Schmidtke², B. Nikutowski^{1,2}, R. Brunner²

¹Institut für Meteorologie, Universität Leipzig, Stephanstr. 3, 04104 Leipzig

²Fraunhofer-Institut für Physikalische Messtechnik (IPM), Heidenhofstraße 8, 79110 Freiburg

Summary

Primary ionisation of major ionospheric constituents is calculated from satellite-borne solar EUV measurements. Number densities of the background atmosphere are taken from the NRLMSISE-00 climatology. From the calculated ionisation rates, an index termed EUV-TEC, which is based on the global total ionisation is calculated, and describes the ionospheric response to solar EUV and its variability. The index is compared against global mean ionospheric total electron content (TEC) derived from GPS data. Results show that the EUV-TEC index provides a better overall representation of global TEC than conventional solar indices like F10.7 do. The EUV-TEC index may be used for scientific research, and to describe the ionospheric effects on radio communication and navigation systems.

1. Introduction

ISO 21348 (ISO, 2007) defines the wavelength range of the EUV radiation between 10 and 121 nm; adjacent wavelength ranges are soft X-rays for shorter and FUV (Far Ultraviolet Radiation) for longer wavelengths. The total amount of EUV energy flux is by about five orders of magnitude smaller than the total solar irradiance integrated over all wavelengths. EUV radiation is completely absorbed at altitudes above 50 km, so that it does not reach neither the troposphere nor the Earth's surface. This absorption occurs mainly in the upper atmosphere (thermosphere) so that EUV radiation is a very important parameter at these heights. The EUV radiation interacts with the atoms and molecules of the upper atmosphere mainly through ionisation, the latter at wavelengths up to 102 nm. Thus, the planetary ionosphere essentially develops through this photoionisation. However, notwithstanding the nature of the primary absorption process (i.e. ionisation, photodissociation), finally the EUV radiation energy is transformed into heat. Thus, EUV radiation is also decisive for the heating of the upper atmosphere.

The EUV radiation is not emitted by the sun at constant rates, but varies on different time scales. An overview of recent measurements and modelling of solar EUV has been provided by Woods (2008). The primary long-term irradiance variability is related to the 11-year Schwabe sunspot cycle. The primary short-term variability is caused by the solar rotation with an average period of 27 days (Carrington rotation period). If there are active regions of the sun, they will also follow this rotation and so they will not always emit their radiation towards the Earth. Solar flare events, associ-

ated with particle eruption events and appearing more frequently during solar maximum than during solar minimum, can affect solar irradiance over a broad wavelength range up to 180 nm. They are short-lived with time scales from minutes to hours. Nevertheless, they cause abrupt changes in density, temperature, and composition of the upper atmosphere.

The solar cycles, and other variability at shorter time scales, affect the absorption and ionisation. Both depend on the incident radiation and the composition of the atmosphere, which is also influenced by the variability of the EUV radiation. Thus, ionospheric changes are strongly related to the variations in the EUV spectral region. Solar, and subsequently upper atmosphere variations can affect the orbits of satellites and spaceships through changes in the drag due to thermospheric density changes. Furthermore, ionospheric fluctuations may cause disturbances of communication and navigation systems (e.g., Pap and Fox 2004).

Solar indices may be used to describe the solar activity. The most frequently used indices are the sunspot number and the solar radio flux F10.7, which is defined as the radio emission from the sun at a wavelength of 10.7 centimetres. However, different indices may be useful to either describe the solar spectrum or the effect of solar EUV on the atmosphere and ionosphere. In this work we present first results to calculate an EUV index for the ionosphere derived from solar EUV radiation measurements, which is intended to describe the ionospheric variability (Schmidtke et al., 2006). This index will be compared with the F10.7 solar radio flux.

2. EUV data

Solar spectra in the wavelength range from 0.1 nm to 200 nm are available from the Solar EUV Experiment (SEE) on board the TIMED satellite. The TIMED mission started in January 2002 with the goal, to observe the Earth's upper atmosphere and the sun simultaneously. TIMED is orbiting the Earth at an altitude of 625 km. Four instruments measure, among others, atmospheric densities, temperatures, winds, ultraviolet emission and solar ultraviolet radiation. SEE is one of these four instruments observing the solar irradiance in the wavelength range from 1 nm to 195 nm using a grating spectrograph and a set of silicon photodiodes (Woods et al., 2000; Woods et al., 2005).

As an example, two spectra from TIMED SEE are shown in Fig. 1. The black line is a spectrum measured near the end of the last solar maximum and the red line represents a spectrum from the last solar minimum, which was very extended. The irradiance variations from solar minimum to solar maximum in the EUV range reach up to 200%. For longer wavelengths this variability decreases rapidly. But in the radio wavelength range at 10.7 cm wavelength as generated in the transition region of the solar atmosphere the solar variability is similar to the variability in the EUV wavelength range, so that the F10.7 radio flux is frequently used as a proxy for solar UV/EUV variability. The total variation of the solar spectrum is only 0.1 to 0.2 % (e.g., Lean et al., 2005).

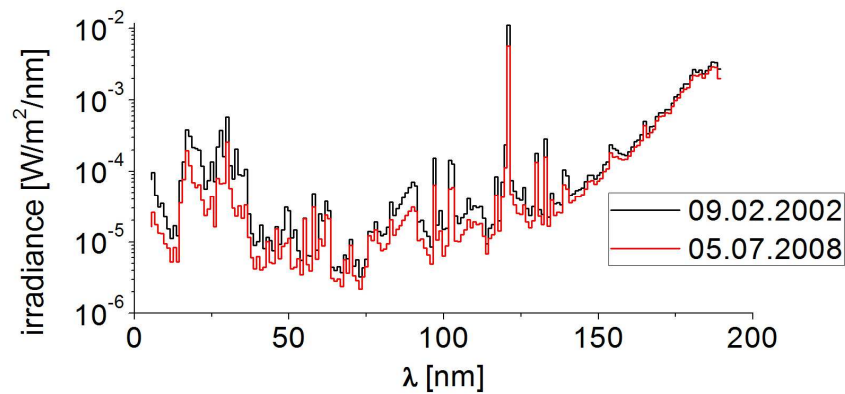


Fig.1: Two examples of EUV spectra as measured by TIMED SEE for solar maximum (black) and minimum (red) conditions.

3. Ionospheric primary ionisation

If EUV radiation meets the upper atmosphere, it interacts with the atmospheric gas. Thus, EUV radiation will be attenuated due to absorption, which in turn is mainly owing to ionisation. The decrease of the radiation can be described by the Lambert-Beer law:

$$dI_E(\lambda) = I_E(\lambda) \cdot \sigma(\lambda) \cdot n \cdot dz, \quad (1)$$

where σ is the absorption cross-section and I_E is the spectral incoming radiation, both dependent on wavelength λ , n is the number density of the absorbing gas, and z is the way through the atmosphere. Note that z does not need to point vertically.

In Fig. 2 the absorption and ionisation cross-sections of four upper atmosphere major constituents, namely atomic oxygen, atomic nitrogen, molecular oxygen and molecular nitrogen, are shown. These cross-sections have been taken from Fennelly and Torr (1992) and Metzger and Cook (1964). The photoionisation cross-sections include multiple ionisation, i.e. possible detachment of more than one electron. Ionisation only occurs at wavelengths up to 102 nm. In the adjacent wavelength range up to 135 nm only the absorption cross-sections for molecular oxygen are shown, because the atomic constituents do not absorb in this region. Huffman (1969) indicates the maximal absorption cross-sections of molecular nitrogen in this region as less than 10^{-25} m^2 , so that they can be neglected. Naturally, both the absorption and ionisation cross-sections of the molecular components are greater than the cross-sections of the atomic components. Furthermore, the absorption cross-sections of the atomic constituents are equal to their ionisation cross-sections, because the atoms can only absorb through ionisation.

The number densities, which are necessary to calculate absorption after Eq. (1), are calculated using the NRLMSISE-00 model (Picone et al., 2002). Fig. 3 (left panel) shows the diurnal averages of the densities for the four important components of the upper atmosphere for different values of solar radio flux, but on the same location

(0°N, 0°E), as predicted by NRLMSISE-00. The day 09.02.2002 represents a day with high solar activity and the 05.07.2008 represents a day with very low solar activity. The influence of the solar activity on the composition of the atmosphere is clearly visible in the model.

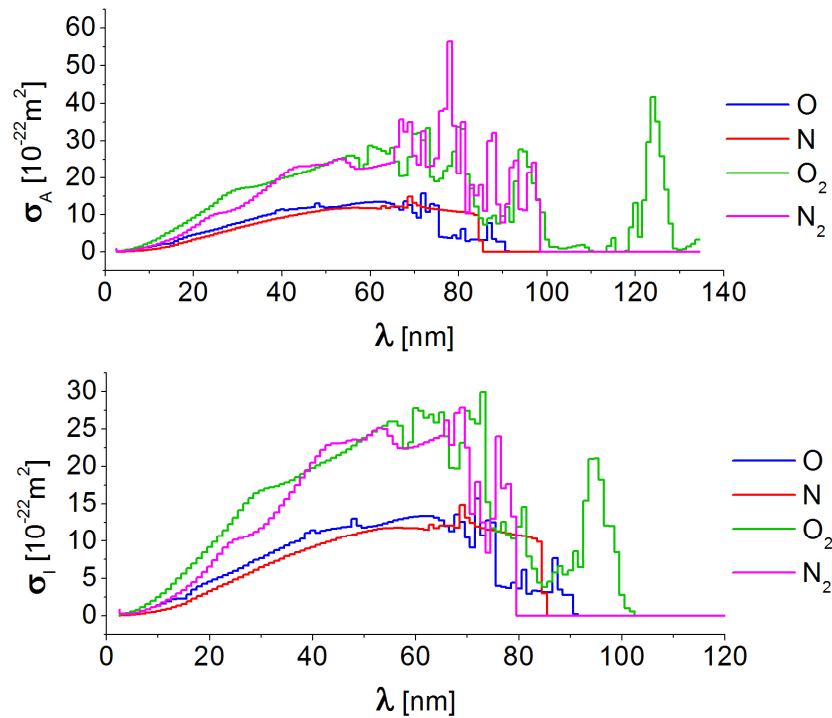


Fig. 2: Absorptions cross-sections (upper panel) and photoionisation cross-sections (lower panel) for four major constituents of the atmosphere. Data taken from Fennelly and Torr (1992) and Metzger and Cook (1964).

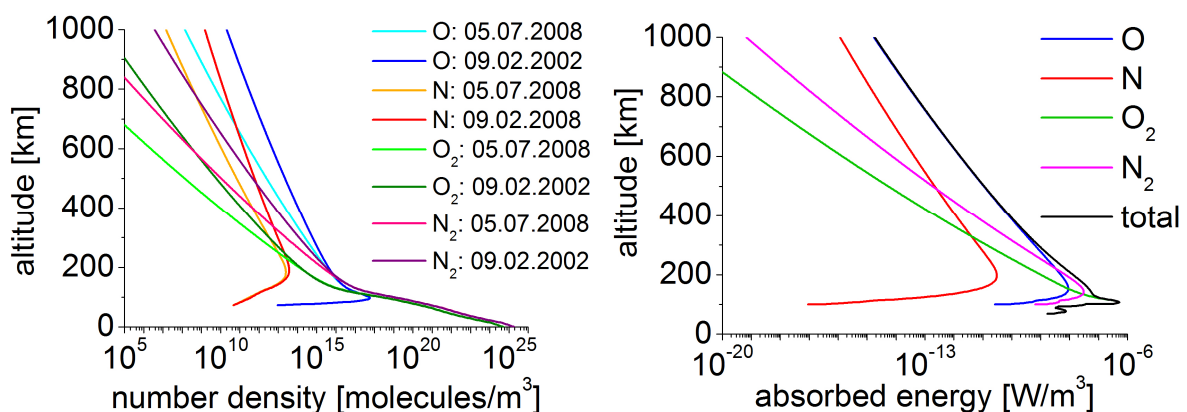


Fig. 3: Left panel: Daily mean NRLMSISE-00 number densities at 0°E, 0°N of four atmospheric gases for different solar activities. Right panel: Absorption profiles on 15.04.2005 for four atmospheric gases calculated for zero zenith angle.

To calculate the absorption and ionisation a model atmosphere is assumed. This atmosphere consists only of the four constituents shown in Fig. 3, and has an altitude of 1000 km. To calculate the absorption, energy deposition and ionisation, essentially Eq. (1) is numerically solved along radiation paths through the atmosphere with a vertical resolution of 1 km. Vertical ionisation profiles are calculated for each latitude and longitude.

The calculation is based on spherical approximations outlined in Fig.4, thereby assuming a spherical atmosphere and a spherical Earth. For each layer, the decrease of the radiation along the radiation path for each single ray must be calculated. To this aim, an angle of entry will be defined, under which the radiation enters the model atmosphere at its upper edge. With this angle the path dS_1 (see Fig. 4) through the uppermost atmospheric layer, and subsequently the absorption and ionisation along this way are calculated. Then the procedure is repeated for the next layer, and then continued until the actual angle corresponds to the zenith angle χ under consideration, providing the spectral radiation energy flux as well as energy deposition at a specific height at a given longitude and latitude. This analysis is then repeated for rays reaching other heights over the grid point under consideration. In this way the absorption and the ionisation are determined for each altitude, and absorption and ionisation profiles will be obtained for a specific zenith angle χ , or a given latitude-longitude grid point at a specific time, respectively.

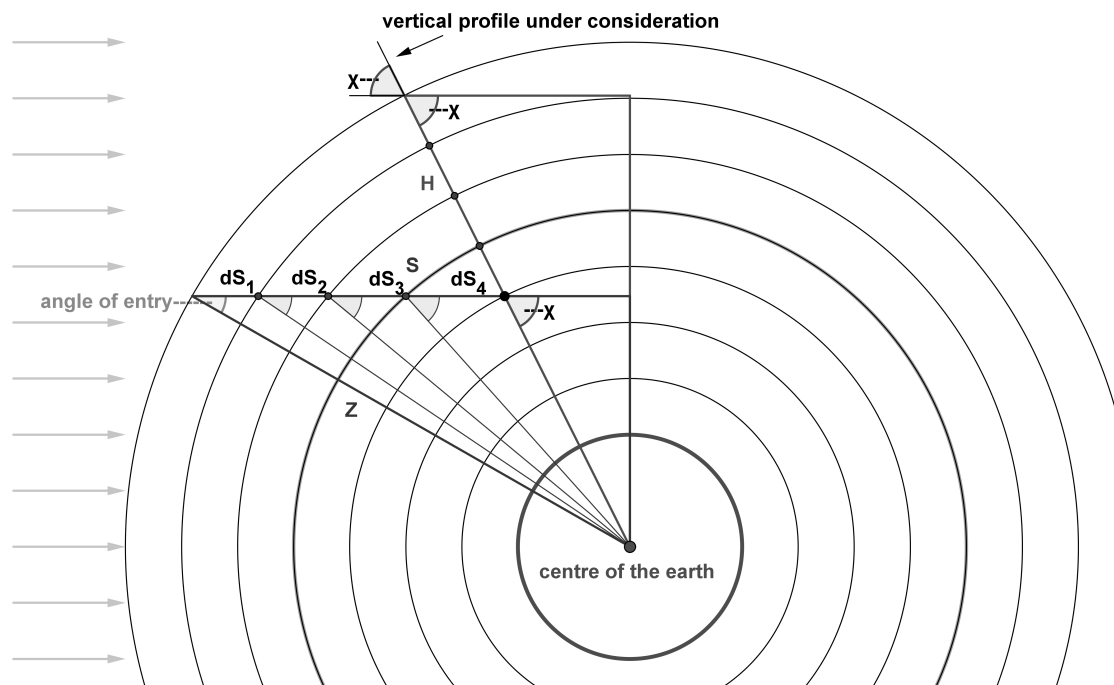


Fig. 4: Sketch of absorption/ionisation calculation for a specific point with given zenith angle.

In Fig. 3 (right panel) the absorption profiles for moderate solar activity for a zero zenith distance on 0°N and 0°E are shown. For altitudes above 300 km absorption through atomic components, especially through atomic oxygen, dominates. The absorption through molecular components prevails at altitudes below 300 km. This is simply owing to the fact that the heavier molecular components dominate at lower altitudes and the lighter atomic components dominate in higher altitudes (see Fig. 3, left panel).

The spectral photon flux density I_{Ph} is calculated from the spectral energy flux density I_{E} divided by the energy of the photons at the respective wavelength:

$$I_{\text{Ph}}(\lambda) = I_{\text{E}}(\lambda) \frac{h \cdot c}{\lambda}, \quad (2)$$

in order to determine the primary ionisation. The assumption is made that only photons contribute to the ionisation. Secondary ionisation processes like photoelectron impact ionisation are neglected. As an example, in Fig. 5 the primary ionisation profiles for moderate solar activity for two different zenith distances on 0°N and 0°E are shown. For $\chi=0^\circ$ the profiles look similar to the absorptions profiles in Fig. 3. For $\chi=100^\circ$ ionisation takes place at much greater altitudes. Because of the preponderance of the atomic constituents at higher altitudes the ionisation for large zenith distances will be dominated by these atomic components.

In the left panel of Fig. 6 the total primary ionisation profiles for four different zenith distances are shown. With increasing χ the altitude of maximum ionisation shifts to greater altitudes and the maximum ion production rate will be smaller. Furthermore, the influence of the ionisation by atomic/molecular constituents increases/decreases. The smaller ion production rates at extremely large zenith angles can be explained by the fact that on the one hand part of the radiation passes the atmosphere without being absorbed. On the other hand, at large χ much absorption already appears before the zenith distance under consideration is reached.

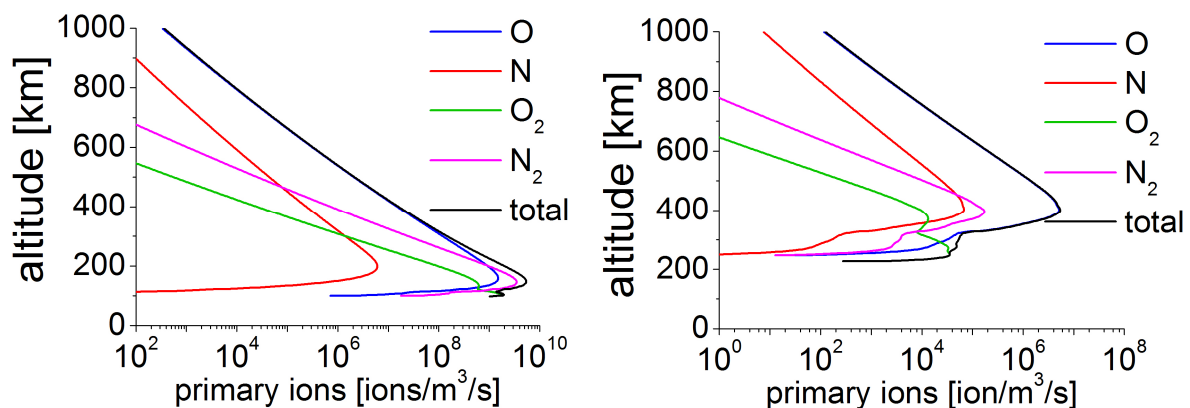


Fig. 5: Primary photoionisation profiles on 15.04.2005 for four atmospheric gases calculated for zero zenith distance $\chi=0^\circ$ (left panel) and $\chi=100^\circ$ (right panel).

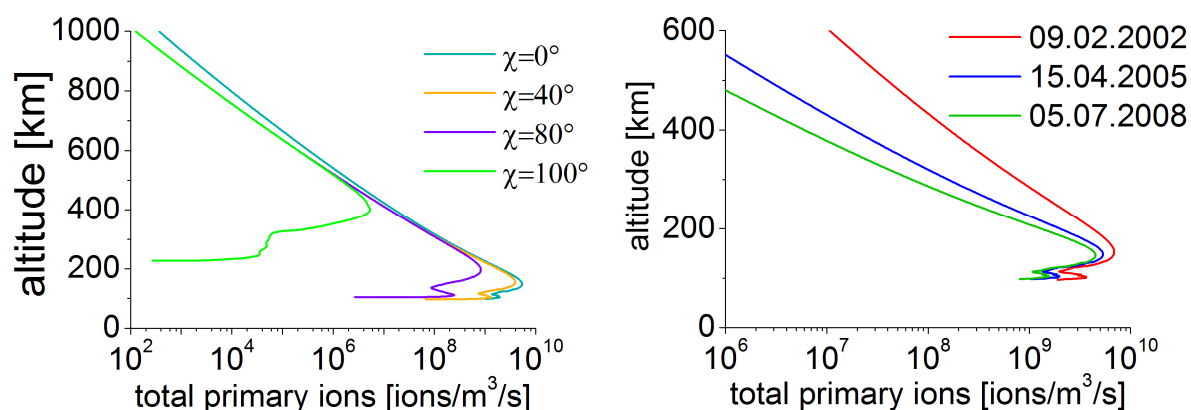


Fig. 6: Primary photoionisation profiles on 15.04.2005 for different zenith distances χ (left panel) and for different solar activities at $\chi=0^\circ$ (right panel).

On the right panel of Fig. 6 the total primary ionisation for zero zenith distance, but for different solar activities are shown. The day 09.02.2002 represents a day of high solar activity, 15.04.2005 represents a day of moderate solar activity and 05.07.2008 is a day of low solar activity. Clearly, the primary ionisation depends on the solar activity. Above 300 km the variability of the ion production rates between solar maximum and solar minimum conditions amounts to one order of magnitude or more. However, the altitude of maximum ionisation shifts only marginally.

4. Results: EUV-TEC index

From the calculated ionisation rates a global ionisation rate is determined through averaging ionisation rates that are calculated for each longitude and latitude on a given day. The single ionisation rate profiles included in this averaging were calculated using global average number densities as input. From these ionisation rates at every grid point a mean global ionisation rate is calculated, and termed EUV-TEC index.

Obviously, ionisation rates may, locally, not be an appropriate measure to describe electron densities, essentially because of the influence of dynamics. However, on a global scale a relatively strong correlation is expected. Thus, in the following the EUV-TEC index will be compared against a global mean Total Electron Content (TEC). To check whether the index is able to describe a considerable part of global ionospheric variability better than existing indices do, global TEC is also compared with the solar radio index F10.7, which is frequently used to describe solar variability.

For the calculation of global TEC, local vertical TEC was used, which is based on a routine evaluation of GPS dual-frequency tracking data (Hernández-Pajares et al. 2009). These data are recorded with the IGS tracking network. The datasets are available every 2 hours for different longitudes and latitudes. To compare the new EUV-

TEC index with global TEC, the local TEC data were weighted with their geographical latitude and then a global diurnal mean was calculated.

In Fig. 7 the time series of EUV-TEC and F10.7, both together with global mean TEC, are shown from 1-JAN-2002 to 31-DEC-2009. A good correlation between EUV-TEC and F10.7 exists during high solar activity. This behaviour is due to the respective origin of the solar EUV flux and the 10.7 cm radio emission. The F10.7 index is originated primarily in the high temperature transition region of the solar atmosphere whereas the solar EUV flux is primarily originated in the chromosphere and to less extend in the transition region and corona. The 10.7 cm radio flux undergoes stronger changes at higher solar activity. During these periods the EUV emissions from higher excited atoms in the solar atmosphere are showing a good correlation with F10.7. As a rule of thumb, the lower the wavelengths of the solar EUV emissions, the higher is their variability with solar activity. In detail, the highly variable FeIX-FeXII lines between 16 nm to about 30 nm are also primarily originated in the solar transition region explaining the stronger correlation at enhanced solar activity.

However, at lower solar activity the EUV emissions from the transition region to a lesser extent contribute to the total EUV activity, hence F10.7 is correlating less strongly with the total EUV radiation during these periods. Consequently, during solar minimum the correlation in Fig. 7 is weaker. Comparing the time series of the EUV-TEC index and global TEC index, however, the seasonal pattern at low solar activity is well visible in both time series. One may conclude that F10.7 does not represent ionospheric variability that well as the EUV-TEC index does, in particular during times of low solar activity.

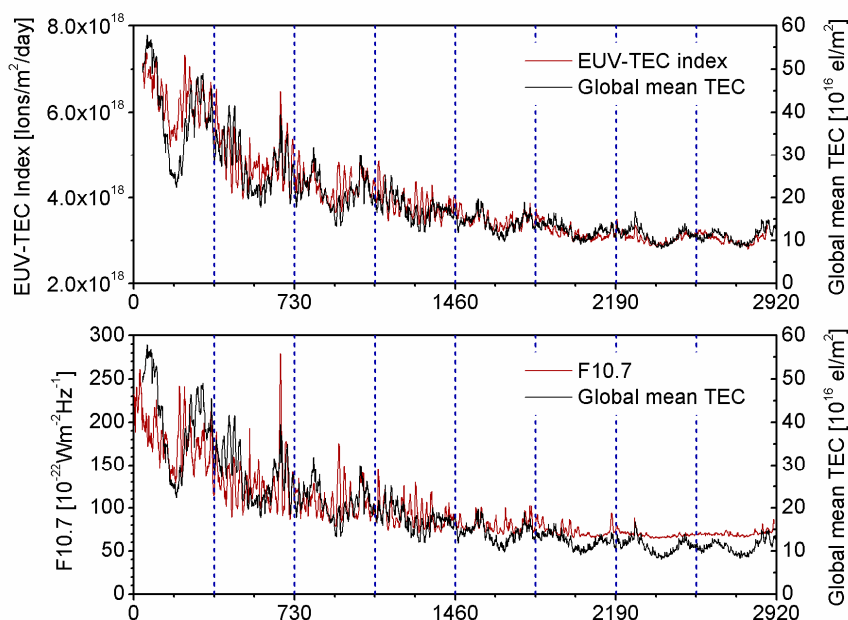


Fig. 7: Time series of daily EUV-TEC indices and global mean TEC (upper panel) and time series for global mean TEC index and F10.7 solar radio flux (lower panel) during 2002 to 2009.

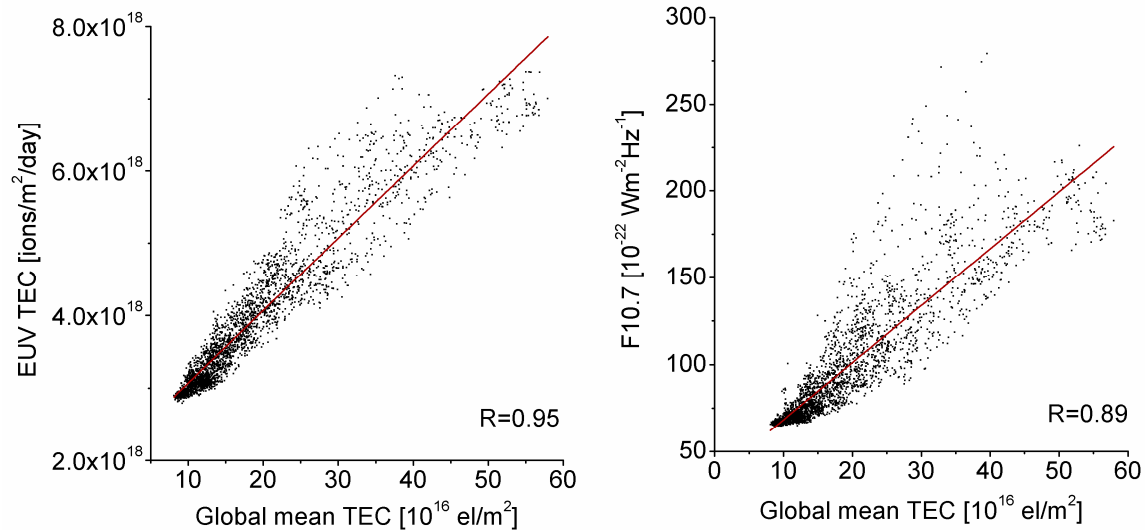


Fig. 8: EUV-TEC index (left panel) and F10.7 (right panel) vs. global mean TEC during 2002 to 2009.

On the left panel of Fig. 8 the EUV-TEC index is compared with the global TEC index from 1.1.2002 to 31.12.2009. There is a strong correlation between these indices with a correlation coefficient of 0.95. In comparison, on the right panel of Fig. 8 the solar radio flux F10.7 is shown vs. the global TEC index. A weaker correlation, with a correlation coefficient of 0.89 only, is obtained. Note that in Figs. 7 and 8 all indices based on the time interval 2002-2009 are compared. Thus, the majority of data points refer to solar minimum conditions rather than during solar maximum conditions, essentially because the last solar minimum was very extended from 2007 to 2009.

5. Conclusions

From solar EUV spectra, global mean primary ionisation rates have been calculated on a daily basis. This provides an index - EUV-TEC -, which to a certain degree describes the influence of solar variability on the ionosphere. Comparison of the index variability with that of global mean TEC provided by GPS measurements show that the index is strongly correlated with TEC. In particular, the index is able to represent the seasonal global TEC cycle during solar minimum, which is not present in other indices used for solar variability description. In particular, for representing ionospheric variability, the new index performs better than the frequently used F10.7 radio flux.

Acknowledgements

TIMED-SEE data has been provided by LASP, University of Colorado, through http://lasp.colorado.edu/see/see_data.html. TEC data has been provided by NASA through <ftp://cdis.gsfc.nasa.gov/gps/products/ionex/YEAR/DOY/>. F10.7 indices have been provided by NGDC through ftp://ftp.ngdc.noaa.gov/STP/SOLAR_DATA/.

References

- Fennelly, J. A., and Torr, D. G., 1992: Photoionization and photoabsorptions cross sections of O, N₂, O₂ and N for aeronomic calculations, *Atomic Data and Nuclear Data Tables*, 51, 321-363.
- Hernández-Pajares, M., Juan, J. M., Sanz, J., Orus, R., Garcia-Rigo, A., Feltens, J., Komjathy, A., Schaer, S. C., and Krankowski, A., 2009: The IGS VTEC maps: a reliable source of ionospheric information since 1998, *J. Geod.*, 83, 263–275.
- Huffman, R. E., 1969: Absorption cross-sections of atmospheric gases for use in aeronomy, *Canadian Journal of Chemistry*, 47, 1823-1834.
- ISO, 2007: ISO 21348:2007(E). Space environment (natural and artificial) — Process for determining solar irradiances, ISO, 12 p.
- Lean, J., Rottmann, G., Harder, J., and Kopp, G., 2005: Source contributions to new understanding of global change and solar variability, *Solar Physics*, 230, 27-53.
- Metzger, P. H. and Cook, G. R., 1964: A reinvestigation of the absorption cross-sections of molecular oxygen in the 1050-1800 Å region, *J. Quant. Spectrosc. Radiat. Transfer.*, 4, 107-116.
- Pap, J. M., and Fox, P., 2004: *Solar Variability and Its Effects on Climate*, American Geophysical Union, 1. Ed., 366 p.
- Picone, J. M., Hedin, A. E., and Drob, D. P., 2002: NRLMSISE-00 empirical model of the atmosphere: Statistical comparisons and scientific issues, *J. Geophys. Res.*, 107, 1468, doi:10.1029/2002JA009430.
- Schmidtke, G., Eparvier, F. G., Solomon, S. C., Tobiska, W. K., and Woods, T. N., 2006: The TIGER (thermospheric-ionospheric geospheric research) program: Introduction, *Adv. Space Res.*, 37, 194-198.
- Woods, T. N., Bailey, S., Eparvier, F., Lawrence, G., Lean, J., McClintock, B., Robie, R., Rottmann, G. J., Solomon, S. C., Tobiska, W. K., and White, O. R., 2000: TIMED Solar EUV Experiment, *Phys. Chem. Earth (C)*, 25, 393-396.
- Woods, T. N., Francis, G. E., Bailey S. M., Chamberlin, P. C., Lean, J., Rottmann, G. J., Solomon, S. C., Tobiska, W. K., and Woodraska, D. L., 2005: Solar EUV Experiment (SEE): Mission overview and first results, *J. Geophys. Res.*, 110, A01312, doi: 10.1029/2004JA010765.
- Woods, T. N., 2008: Recent advances in observations and modeling of the solar ultraviolet and X-ray spectral irradiance, *Adv. Space Res.*, 42, 895-902.